JPE 17-1-18

https://doi.org/10.6113/JPE.2017.17.1.181
ISSN(Print): 1598-2092 / ISSN(Online): 2093-4718

Design of a Hybrid Controller for the Three-phase Four-leg Voltage-source Inverter with Unbalanced Load

Van-Tuan Doan*, Ki-Young Kim*, Woojin Choi†, and Dae-Wook Kim**

*,†Department of Electrical Engineering, Soongsil University, Seoul, Korea
**Department of Economics, Soongsil University, Seoul, Korea

Abstract

The three-phase four-leg voltage-source inverter topology is an interesting option for the three-phase four-wire system. With an additional leg, this topology can achieve superior performance under unbalanced and nonlinear load conditions. However, because of the low bandwidth of conventional controllers in high-power inverter applications, the system cannot guarantee a balanced output voltage under the unbalanced load condition. Most of the methods proposed to solve this problem mainly use the multiple synchronous frame method, which requires several controllers and a large amount of computation because of frame transformation. This study proposes a simple hybrid controller that combines proportional–integral (PI) and resonant controllers in the synchronous frame synchronized with the positive-sequence component of the output voltage of the three-phase four-leg inverter. The design procedure for the controller and the theoretical analysis are presented. The performance of the proposed method is verified by the experimental results and compared with that of the conventional PI controller.

Key words: Hybrid controller, Resonant controller, Three-phase four-leg voltage-source inverter, Unbalanced load condition

I. INTRODUCTION

In three-phase distributed power generation systems, the inverter is often connected to the load, which requires four wires, including a neutral one. In this case, the power system can provide the neutral wire in two ways: via a conventional three-phase inverter with a Δ-Y connected isolation transformer or a three-phase four-wire inverter. However, considering that the conventional three-phase inverter with an isolation transformer exhibits many disadvantages, such as bulkiness, large weight, and high cost, three-phase four-wire transformerless topologies are preferred [1]-[5]. Three-phase four-wire inverters can be divided into three-leg inverters with a split DC link and four-leg inverters [6]-[11]. The split DC-link capacitor topology requires only six power switches because the neutral current path is provided by the midpoint of the DC link. However, this topology possesses high DC-link voltage and large DC-link capacitance. In the three-phase four-leg topology (shown in Fig. 1), the neutral wire is provided by the additional fourth leg. This topology exhibits important advantages, such as compactness, fast response, small DC-link capacitance, and a higher modulation index than its split DC link counterpart [11].

Several strategies have been developed to control three-phase four-leg inverters [12]-[21]. One of the popular methods is the proportional–integral (PI) controller employed to regulate the fundamental component of output voltage [12], [14]-[16]. The PI controller can be easily implemented either in the rotating [12], [15], [16] or stationary [13], [14] frame. Given that the PI controller has a large gain at DC mode, it demonstrates good performance under balanced load conditions. With regard to inverters for high-power applications, the pulse-width modulation (PWM) frequency is limited to several kHz to reduce switching losses, and a low-pass filter is adopted for the output of these inverters. The resonant frequency of the output filter is typically lower than several hundred Hertz because the resonant frequency of the output filter should be between the fundamental output and switching frequencies. Under light loads, the double pole of the LC output filter introduces a large resonant peak and a steep

Manuscript received Jul. 26, 2016; accepted Nov. 22, 2016
Recommended for publication by Associate Editor Trillion Q. Zheng.
†Corresponding Author: cwj777@ssu.ac.kr
Tel: +82-2-820-0652, Fax: +82-2-817-7961, Soongsil University
*Dept. of Electrical Engineering, Soongsil University, Korea
**Dept. of Economics, Soongsil University, Korea

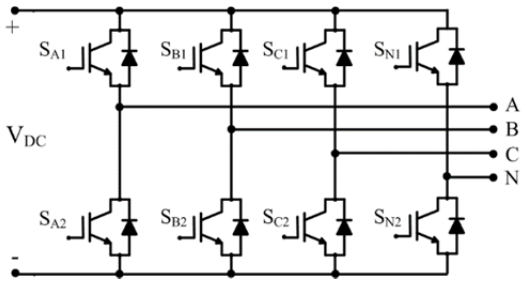

Fig. 1. Three-phase four-leg inverter topology.

phase change. Consequently, the bandwidth of the inverter is limited to a value lower than the resonant frequency of the output filter to guarantee system stability. With such a low bandwidth, the PI controller exhibits a poor transient response and poor regulation performance when AC quantities occur as a result of the unbalanced current. To improve transient performance, complex controllers, such as the linear quadratic regulator [12] or the pole placement method, must be used [17]. Although both methods are complex, none of them can effectively solve the unbalanced load problem. In [18], a predictive controller was used to directly select the most suitable switching vector with the minimum cost function. However, the method involves a large amount of computation and is incompatible with the space vector modulation technique.

Various solutions based on symmetrical components have been proposed to address the unbalanced load problem [19]-[25]. In these methods, the unbalanced voltage is decomposed into a set of symmetrical components, namely, positive-sequence, negative-sequence, and zero-sequence components. Hence, the unbalanced voltage can be compensated by the control of each symmetrical voltage set. By applying appropriate rotating coordinate transformation to the symmetric components, the conventional PI controller can be utilized to generate balanced output waveforms under unbalanced load conditions. However, this procedure requires a large amount of computation because of the complexity of calculating the symmetric components, coordinate transformation, and controllers [19], [20], [22], [24]. In [19], a zero-damping band-pass filter was employed in the 0 channel to reduce the number of rotating frames. However, coordinate transformation can only be eliminated in the 0 channel. In [20], a negative-sequence voltage compensator (NVC) and a harmonic voltage compensator (HVC) were applied; as a result, the controller in NVC was able to operate with pure DC control variables, and leading angle information was not required in HVC. Zero-sequence voltage distortion can be compensated by an output transformer with delta-wye winding. However, given the low-frequency transformer in the topology, this approach is used only for several specific applications. In [23], sequence decomposition of voltage and current was implemented digitally through phasor representation. The proposed digital control scheme was used to obtain DC signals for all symmetrical components. However, the overall control scheme is complex.

In the current study, a novel hybrid controller composed of PI and resonant controllers in the synchronous frame was developed for the three-phase four-leg inverter to provide balanced three-phase voltages under unbalanced loads. The proposed hybrid controller has a unique characteristic: it has an infinity gain at both DC and desired frequencies. It can be used for multiple harmonics control, as shown in previous studies [25], [26]. When the three-phase four-leg inverter bears unbalanced load, negative- and zero-sequence voltages appear as AC noises in the rotating frame synchronized with a positive-sequence component. Hence, the inverter can generate a balanced three-phase output voltage by selecting a suitable resonant frequency for the resonant controller to mitigate the noises. The proposed method is simple and effective because it requires low-bandwidth controllers, a small number of controllers, and a small amount of computation.

II. Proposed Hybrid Controller for the Three-Phase Four-Leg Inverter

The structure of the proposed hybrid controller (PI–resonant or PI-R) is shown in Fig. 2. The controller is implemented by combining PI and resonant controllers in the rotating frame synchronized with a positive-sequence component of output voltage. For simplicity, the rotating frame synchronized with a positive-sequence component is referred to merely as “rotating frame” in the rest of the paper. The PI controller has a high gain at DC mode, which guarantees a zero steady-state error of output voltage. The resonant controller is designed to provide a high gain at desired frequencies to suppress the unwanted noises caused by the unbalanced load.

The transfer function of the proposed controller is expressed as

$$C(s) = K_p + \frac{K_I}{s} + \frac{K_R s}{s^2+\omega_0^2}. \quad (1)$$

The hybrid controller exhibits the combined characteristics of PI and resonant controllers because it has one real zero and two complex zeroes in its transfer function. These complex zeroes introduce a notch below resonant frequency ω_0.

A control block diagram of the proposed hybrid controller is shown in Fig. 3. The control of the proposed hybrid controller is similar to the conventional feedback control of the inverter. The output voltages are measured and transformed into rotating frame dq0. In the dq0 coordinate, three hybrid controllers are used to regulate the output voltage independently in each channel (d, q, and 0). To obtain the sinusoidal output voltage, the negative- and zero-sequence components need to be set to zero. The balanced component in the output voltage is regulated by the

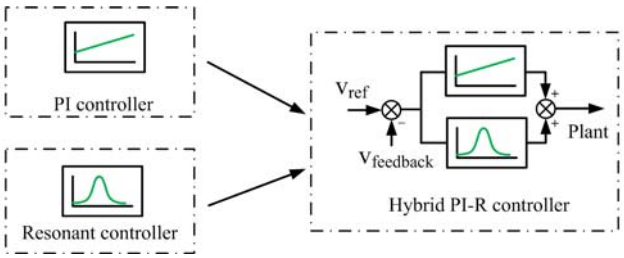

Fig. 2. Proposed hybrid controller.

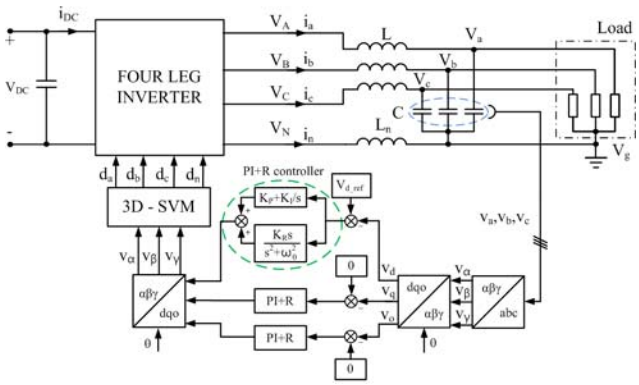

Fig. 3. Control block diagram of the proposed controller for the three-phase four-leg inverter.

TABLE I
COMPARISON OF THE PROPOSED CONTROLLER WITH OTHER CONTROLLERS

	In [19]	In [20]	In [23]	Proposed controller
Number of voltage controllers	5	3	9	3
Sequence decomposition /composition	No	Yes	Yes	No
Number of rotating-frame transformation	4	4	6	2

PI controller, and the unbalanced component is controlled by the resonant controller. The outputs of the controllers are inversely transformed into the αβγ coordinate, and the gate signals for the power switches are generated by applying 3D space vector modulation (3D SVM). The proposed controller requires fewer controllers and less computation than those proposed in [19], [20], and [23]. The advantages of the proposed controller become evident when it is compared with other previous methods (Table I).

III. DESIGN OF THE PROPOSED HYBRID CONTROLLER FOR THE THREE-PHASE FOUR-LEG INVERTER WITH UNBALANCE LOAD

The average model of the three-phase four-leg inverter and an analysis of the unbalanced load current in the rotating frame are presented in this section. The design challenge is the use of the conventional method to design the controller under an unbalanced load condition. The design procedure of the proposed hybrid controller is also presented in this section.

A. Average Model of the Three-phase Four-leg Inverter

Given the nonlinearity of the switch network model, its average model is used to design the controller with effectiveness and ease. By defining duty ratio d_k (k = A, B, C, N), which represents the average time of a leg during a switching period, the output voltage and the DC-link current can be expressed by linear equations (2) and (3), respectively [11].

$$[V_{AN} \quad V_{BN} \quad V_{CN}]^T = [d_{AN} \quad d_{BN} \quad d_{CN}]^T.V_{DC}, \tag{2}$$

$$i_{DC} = [d_{AN} \quad d_{BN} \quad d_{CN}][i_a \quad i_b \quad i_c]^T, \tag{3}$$

where $[V_{AN} \quad V_{BN} \quad V_{CN}]$ is the output phase voltage vector, $[d_{AN} \quad d_{BN} \quad d_{CN}]$ is the line-to-neutral duty ratio vector, $[i_a \quad i_b \quad i_c]$ is the output current vector, and V_{DC} and i_{DC} are the DC-link voltage and current, respectively.

To attenuate the high-order harmonics caused by PWM, the second-order LC filter is typically used for inverters operating in the standalone mode. The average model of the three-phase four-leg inverter, including the output LC filter, is shown in Fig. 4. Its state-space model is expressed in Equations (4), (5), and (6).

$$\frac{d}{dt}\begin{bmatrix} I_a \\ I_b \\ I_c \end{bmatrix} = \frac{L_n}{L}\frac{d}{dt}\begin{bmatrix} I_n \\ I_n \\ I_n \end{bmatrix} + \frac{V_{DC}}{L}\begin{bmatrix} d_{AN} \\ d_{BN} \\ d_{CN} \end{bmatrix} - \frac{1}{L}\begin{bmatrix} V_a \\ V_b \\ V_c \end{bmatrix}, \tag{4}$$

$$\frac{d}{dt}\begin{bmatrix} V_a \\ V_b \\ V_c \end{bmatrix} = \frac{1}{C}\left\{\begin{bmatrix} I_a \\ I_b \\ I_c \end{bmatrix} - \begin{bmatrix} I_{La} \\ I_{Lb} \\ I_{Lc} \end{bmatrix}\right\}, \tag{5}$$

$$I_a + I_b + I_c = I_n, \tag{6}$$

where I_{La}, I_{Lb}, and I_{Lc} are the load currents of phases A, B, and C, respectively.

Equations (4) to (6) show that the three-phase four-leg inverter is a sixth-order system with AC variables.

By applying Park's transformation in Equation (7) to Equations (4) to (6), the state variable of the current $[i_d \quad i_q \quad i_0]$ and that of the voltage $[V_d \quad V_q \quad V_o]$ in dq0 coordinates can be represented by Equations (8) and (9), respectively.

$$T_2 = \frac{2}{3}\begin{bmatrix} cos\omega t & cos\left(\omega t - \frac{2}{3}\pi\right) & cos\left(\omega t + \frac{2}{3}\pi\right) \\ -sin\omega t & -sin\left(\omega t - \frac{2}{3}\pi\right) & -sin\left(\omega t + \frac{2}{3}\pi\right) \\ \frac{1}{2} & \frac{1}{2} & \frac{1}{2} \end{bmatrix} \tag{7}$$

$$\frac{d}{dt}\begin{bmatrix} I_d \\ I_q \\ I_0 \end{bmatrix} = \begin{bmatrix} 0 & \omega & 0 \\ -\omega & 0 & 0 \\ 0 & 0 & 0 \end{bmatrix}\begin{bmatrix} I_d \\ I_q \\ I_0 \end{bmatrix} + V_{DC}\begin{bmatrix} \frac{1}{L} & 0 & 0 \\ 0 & \frac{1}{L} & 0 \\ 0 & 0 & \frac{1}{L+3L_n} \end{bmatrix}\begin{bmatrix} d_d \\ d_q \\ d_0 \end{bmatrix}$$

$$-\begin{bmatrix} \frac{1}{L} & 0 & 0 \\ 0 & \frac{1}{L} & 0 \\ 0 & 0 & \frac{1}{L+3L_n} \end{bmatrix}\begin{bmatrix} V_d \\ V_q \\ V_0 \end{bmatrix} \tag{8}$$

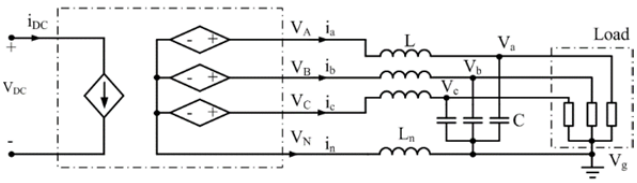

Fig. 4. Average model of the three-phase four-leg inverter.

$$\frac{d}{dt}\begin{bmatrix}V_d\\V_q\\V_0\end{bmatrix}=\begin{bmatrix}0&\omega&0\\-\omega&0&0\\0&0&0\end{bmatrix}\begin{bmatrix}V_d\\V_q\\V_0\end{bmatrix}+\frac{1}{C}\left\{\begin{bmatrix}I_d\\I_q\\I_0\end{bmatrix}-\begin{bmatrix}I_{Ld}\\I_{Lq}\\I_{L0}\end{bmatrix}\right\} \quad (9)$$

By rearranging Equations (8) and (9), the state-space model of the three-phase four-leg inverter in the rotating frame is provided by Equations (10) and (11). Equation (10) shows that the 0 channel is independent of the other channels. However, cross-coupling terms exist between d and q channels. Thus, the system in the rotating frame can be decomposed into a fourth-order multi-input multi-output model for d and q channels and into a conventional second-order model for the 0 channel.

$$\frac{d}{dt}\begin{bmatrix}I_d\\V_d\\I_q\\V_q\\I_0\\V_0\end{bmatrix}=\begin{bmatrix}0&1/C&\omega&0&0&0\\-1/L&0&0&\omega&0&0\\-\omega&0&0&1/C&0&0\\0&-\omega&-1/L&0&0&0\\0&0&0&0&0&1/C\\0&0&0&0&-1/(L+3L_n)&0\end{bmatrix}\begin{bmatrix}I_d\\V_d\\I_q\\V_q\\I_0\\V_0\end{bmatrix}+\begin{bmatrix}0&0&0\\\frac{V_{DC}}{L}&0&0\\0&0&0\\0&\frac{V_{DC}}{L}&0\\0&0&0\\0&0&\frac{V_{DC}}{L+3L_n}\end{bmatrix}\begin{bmatrix}d_d\\d_q\\d_0\end{bmatrix}+\begin{bmatrix}-1/C&0&0\\0&0&0\\0&-1/C&0\\0&0&0\\0&0&-1/C\\0&0&0\end{bmatrix}\begin{bmatrix}I_{Ld}\\I_{Lq}\\I_{L0}\end{bmatrix} \quad (10)$$

$$\begin{bmatrix}V_d\\V_q\\V_0\end{bmatrix}=\begin{bmatrix}1&0&0&0&0&0\\0&0&1&0&0&0\\0&0&0&0&1&0\end{bmatrix}\begin{bmatrix}V_d\\I_d\\V_q\\I_q\\V_0\\I_0\end{bmatrix}+\begin{bmatrix}0&0&0\\0&0&0\\0&0&0\end{bmatrix}\begin{bmatrix}d_d\\d_q\\d_0\end{bmatrix} \quad (11)$$

Given that the coupling terms on the d and q channels can be eliminated with the feed-forward technique [7], the state model for the d channel can be expressed as

$$\frac{d}{dt}\begin{bmatrix}V_d\\I_d\end{bmatrix}=\begin{bmatrix}0&1/C\\-1/L&0\end{bmatrix}\begin{bmatrix}V_d\\I_d\end{bmatrix}+\begin{bmatrix}0\\V_{DC}/L\end{bmatrix}d_d+\begin{bmatrix}-1/C\\0\end{bmatrix}I_{Ld}. \quad (12)$$

Hence, the control-to-output transfer function on the d channel is

$$G_d(s)=\frac{V_d}{d_d}=\frac{V_{DC}}{LCs^2+\left(\frac{L}{R_{Load}}\right)s+1} \quad (13)$$

The system model on the q channel is similar to that on the d channel. Meanwhile, the control-to-output voltage transfer function on the 0 channel is different and has a lower resonant frequency, as shown in Equation (14).

$$G_o(s)=\frac{V_o}{d_o}=\frac{V_{DC}}{(L+3L_n)Cs^2+\left(\frac{L+3L_n}{R_{Load}}\right)s+1} \quad (14)$$

Typically, the second-order LC output filter of the inverter is designed to have −40 dB/dec attenuation at high frequencies, and its resonant frequency is set between the switching and fundamental frequencies of output voltage by Equation (15).

$$\omega_{res}=\frac{1}{\sqrt{LC}} \quad (15)$$

In this study, the resonant frequency of the output filter was set to 1 kHz. The design parameters of the inverter are shown in Table II.

TABLE II
SPECIFICATIONS OF THE INVERTER

Parameter	Symbol	Value
Rated power	P_o	3 kW
Output line–line voltage	V_{o_ll}	220 V
Output frequency	f_o	60 Hz
DC-link voltage	V_{DC}	400 V
PWM frequency	f_{PWM}	10 KHz
Output inductor of phases A, B, C	L	2.5 mH
Output inductor of neutral phase	L_n	1.2 mH
Output capacitor	C	10 μF

The Bode plots for the d and 0 channels of the inverter are shown in Figs. 5 and 6, respectively. Figs. 5 and 6 indicate that the control-to-output transfer functions on the d and 0 channels show the characteristics of a damped second-order system with full load. However, the resonant peak and phase reversal occur at the resonant frequency when the load is light. This phenomenon becomes severe when the digital controller is used because the phase lag caused by the controller is added to the system; this can cause system instability.

B. Analysis of Unbalanced Load Current in the Rotating Frame

Under the unbalanced load condition, the load voltage can be decomposed into symmetric components, as shown in Equation (16).

$$\begin{bmatrix}I_{La}\\I_{Lb}\\I_{Lc}\end{bmatrix}=\begin{bmatrix}I_{Lap}\\I_{Lbp}\\I_{Lcp}\end{bmatrix}+\begin{bmatrix}I_{Lan}\\I_{Lbn}\\I_{Lcn}\end{bmatrix}+\begin{bmatrix}I_{Lao}\\I_{Lbo}\\I_{Lco}\end{bmatrix}, \quad (16)$$

where the positive-, negative-, and zero-sequence currents are expressed by Equations (17), (18), and (19), respectively.

$$\begin{bmatrix}I_{Lap}\\I_{Lbp}\\I_{Lcp}\end{bmatrix}=I_{Lpp}\begin{bmatrix}cos(\omega t+\varphi_p)\\cos(\omega t+\varphi_p-2\pi/3)\\cos(\omega t+\varphi_p+2\pi/3)\end{bmatrix}, \quad (17)$$

$$\begin{bmatrix}I_{Lan}\\I_{Lbn}\\I_{Lcn}\end{bmatrix}=I_{Lnp}\begin{bmatrix}cos(\omega t+\varphi_n)\\cos(\omega t+\varphi_n+2\pi/3)\\cos(\omega t+\varphi_n-2\pi/3)\end{bmatrix}, \quad (18)$$

$$\begin{bmatrix}I_{Lao}\\I_{Lbo}\\I_{Lco}\end{bmatrix}=I_{Lop}\begin{bmatrix}cos(\omega t+\varphi_o)\\cos(\omega t+\varphi_o)\\cos(\omega t+\varphi_o)\end{bmatrix}, \quad (19)$$

where I_{Lpp}, I_{Lnp}, and I_{Lop} are peak values and φ_p, φ_n, and φ_o are phase angles.

By applying Park's transformation in Equation (7) to Equations (17), (18), and (19), the symmetric components of the load current in the synchronous frame can be expressed by Equations (20) to (22).

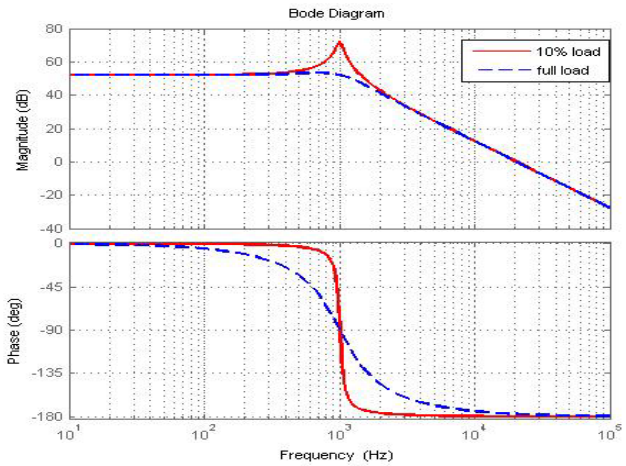

Fig. 5. Bode plots of the d channel under light load (solid line) and full load (dashed line).

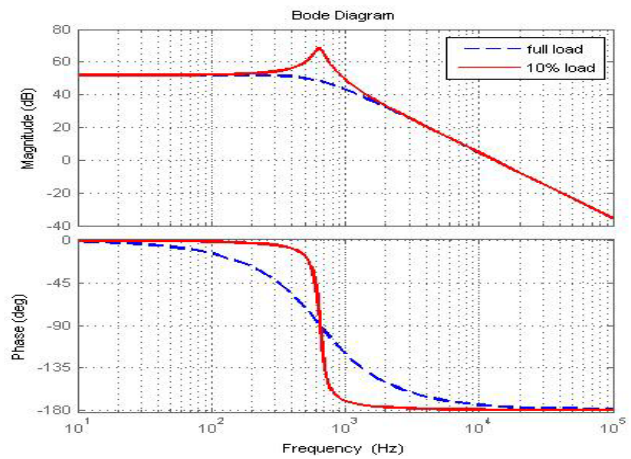

Fig. 6. Bode plot of the 0 channel under light load (solid line) and full load (dashed line).

$$\begin{bmatrix} I_{Ldp} \\ I_{Lqp} \\ I_{Lop} \end{bmatrix} = I_{Lpp} \begin{bmatrix} cos\,\varphi_p \\ -sin\varphi_p \\ 0 \end{bmatrix} \quad (20)$$

$$\begin{bmatrix} I_{Ldn} \\ I_{Lqn} \\ I_{Lon} \end{bmatrix} = I_{Lnp} \begin{bmatrix} cos(2\omega t + \varphi_n) \\ cos(2\omega t - \varphi_n) \\ 0 \end{bmatrix} \quad (21)$$

$$\begin{bmatrix} I_{Lao} \\ I_{Lbo} \\ I_{Lco} \end{bmatrix} = I_{Lop} \begin{bmatrix} 0 \\ 0 \\ cos(\omega t + \varphi_o) \end{bmatrix} \quad (22)$$

Equations (20) to (22) indicate that in the unbalanced load condition, negative- and zero-sequence currents appear as harmonics with 2 ω frequency on the d and q channels and with ω frequency on the 0 channel, respectively.

C. *Challenges in Designing the Controller for the Three-phase Four-leg Inverter under Unbalanced Load Condition*

Given that the transfer functions of the three-phase four-leg inverter in the rotating frame are second-order systems as shown in Equations (13) and (14), a simple linear controller should be used to regulate the output voltage. However, the main challenge in the design is the resonant peak of the second-order system under light load. To guarantee system stability, the bandwidth is extended beyond the resonant frequency or reduced to much lower than the resonant frequency. The former is difficult for high-power applications because of the low switching frequency. The parameters in Table II show that the poles/zero frequencies of the controller needs to be limited to 5 kHz because the switching frequency is 10 kHz [27]. In the typical design of the controller, the pole and zero are placed to attenuate the high-frequency components and increase the phase margin. However, the effects of the pole and zero cancel each other because they cannot be located far enough from each other in this case [28]. Meanwhile, the latter can be implemented by using the PI controller. Fig. 7 shows the design of the PI controller for the d channel in the frequency domain. To consider the phase delay caused by the digital control, a time delay is added to the transfer functions of d, q, and 0 channels [29]. With the addition of this time delay, the phase change of the system at the resonant peak becomes severe. At the resonant peak, the phase curve crosses -180°, and the system has a minimum gain margin. Given that the phenomenon is the worst at light load, the controller needs to be designed by considering the stability criterion in this condition. Thus, in the asymptote design method, the open-loop system gain at the resonant peak should be the sum of the resonant peak and the gain margin. The crossover frequency of the open-loop system at several ten Hertz can be determined by assuming a −20 dB/dec slope. As mentioned in the previous section, the negative-sequence component appears at 120 Hz. Thus, the PI controller is unable to compensate for this noise generated by the unbalanced load. To guarantee a balanced output voltage under the unbalanced load condition, another controller needs to be added to compensate for the low-frequency component. The design of the hybrid controller is discussed in the following section.

D. *Design of the Hybrid Controller for the Three-phase Four-leg Inverter under Unbalanced Load*

First, the PI controller for each channel was designed in the frequency domain to achieve the desired stability margin by using a conventional design procedure. The parameters of the PI controller for each channel are shown in Table 3. To guarantee the stability of the system under light load, the gain margin was set to 14.2 dB. The bandwidth of the d and q channels was 13.4 Hz and that of the 0 channel was 10 Hz. Hence, the phase margin of each channel was at approximately 90°, which is sufficient for system stability. The pole–zero map of the d channel and the PI controller is shown in Fig. 8.

Second, the resonant controller was designed. The resonant frequency of the controller, ω_o, was set to the same frequency of the negative sequence on d and q channels and of the zero sequence on the 0 channel. The Bode plots of the hybrid controller with different values of resonant gain are shown in

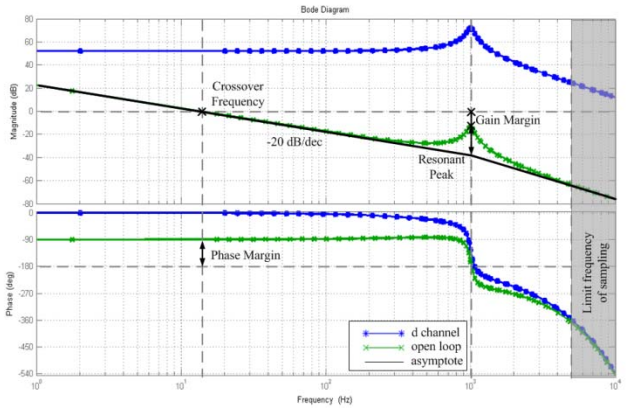

Fig. 7. Design of the PI controller for the d channel.

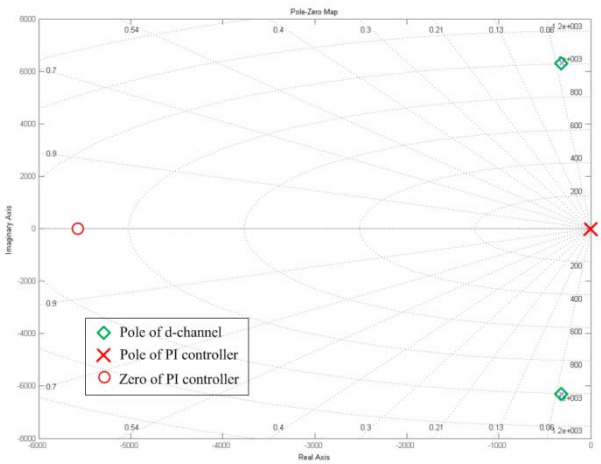

Fig. 8. Pole–zero map of the d channel and PI controller.

TABLE III
PARAMETERS OF THE PI CONTROLLER FOR EACH CHANNEL

	K_i	K_p	Gain margin (dB)	Phase margin (degree)	Crossover frequency (Hz)
d channel	0.21	3.78×10^{-5}	14.2	90.3	13.4
q channel	0.21	3.78×10^{-5}	14.2	90.3	13.4
0 channel	0.16	4.59×10^{-5}	16	90.6	10

Fig. 9. When the resonant controller is combined with the PI controller, a pair of complex zeroes is introduced below the resonant frequency and shifts the real zero to the high-frequency region. Thus, the gain margin set by the PI controller previously is reduced, and a trade-off between the bandwidth of the resonant controller and the gain margin of the open loop is introduced in the design.

Fig. 10 shows the Bode plots of the d channel, hybrid controller, and loop gain of system. For a digital implementation, the controller needs to be discretized. The resonant controller has highly selective characteristics and is seriously affected by the discretization method [30]. Thus, Tustin approximation with frequency pre-warping (23) was used to ensure the matching of the continuous and discrete time frequencies at the resonant frequency.

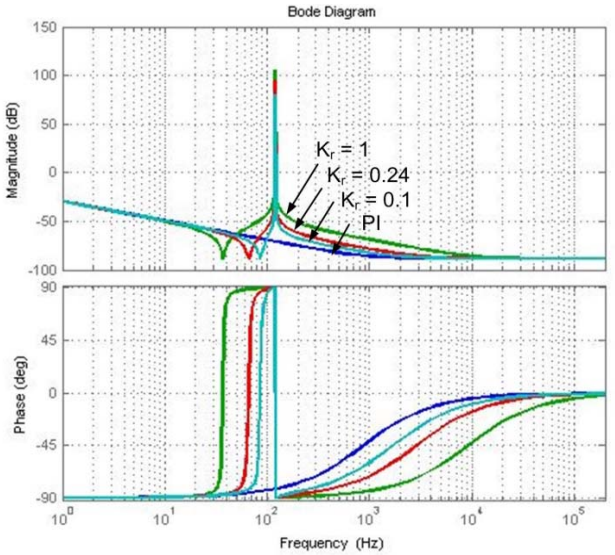

Fig. 9. Bode plots of the hybrid controller with different Kr values ($K_P = 3.78\times10^{-5}$, $K_I = 0.21$).

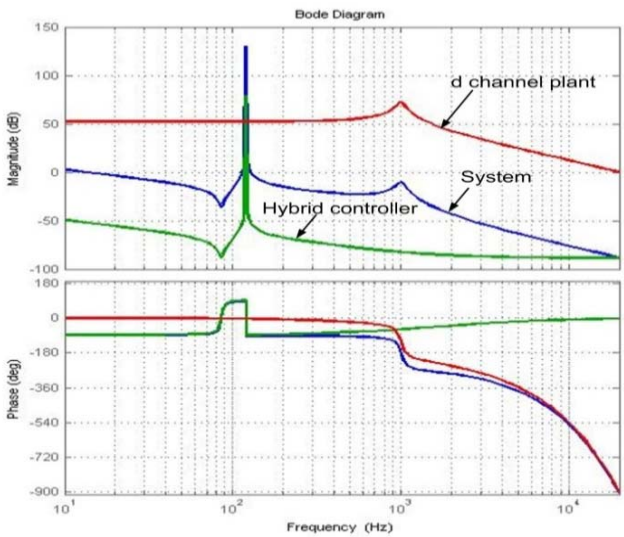

Fig. 10. Bode plot of the d channel with the hybrid controller.

$$s = \frac{\omega_o}{tan\left(\frac{\omega_o T_s}{2}\right)} \frac{z-1}{z+1} \quad (23)$$

IV. EXPERIMENTAL RESULTS

A 3 kW prototype three-phase four-leg inverter with the design parameters shown in Table II was built to verify the proposed controller (Fig. 11). The 3D SVM algorithm and the proposed hybrid controllers were implemented in DSP F28335. To prove the superior performance of the proposed hybrid controller, its performance was tested under both balanced and unbalanced loads. The results were compared with those of the conventional PI controller. As shown in Fig. 12, under balanced three-phase loads, the output phase voltages are balanced, and a small neutral current exists. Fig. 13 shows the output voltage waveforms under unbalanced load conditions. Fig. 13(a) shows the unbalanced output

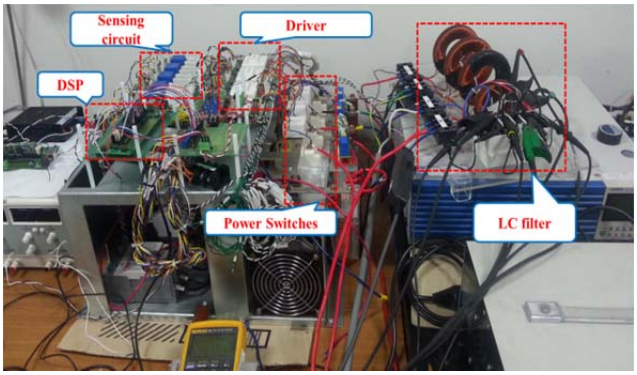

Fig. 11. Experimental setup of a 3 kW three-phase four-leg inverter.

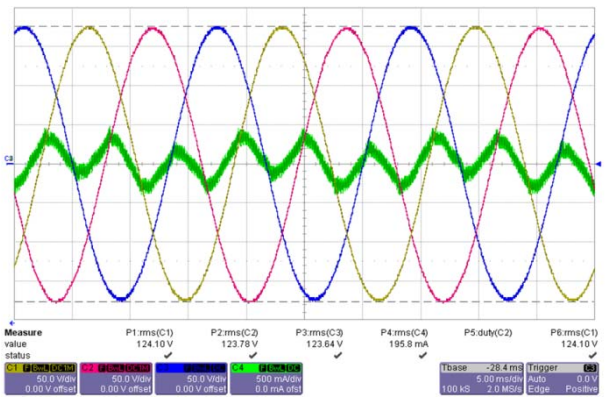

Fig. 12. Output phase voltage waveforms under balanced load with the proposed hybrid controller.

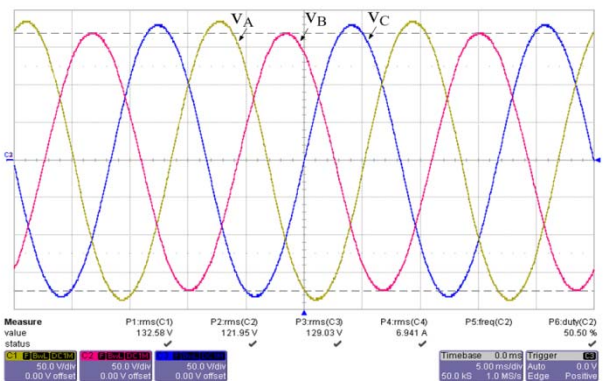

(a) Output phase voltage waveforms with the conventional PI controller.

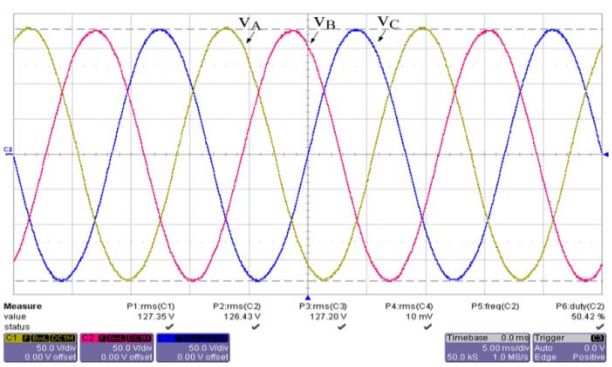

(b) Output phase voltage waveforms with the proposed hybrid controller.

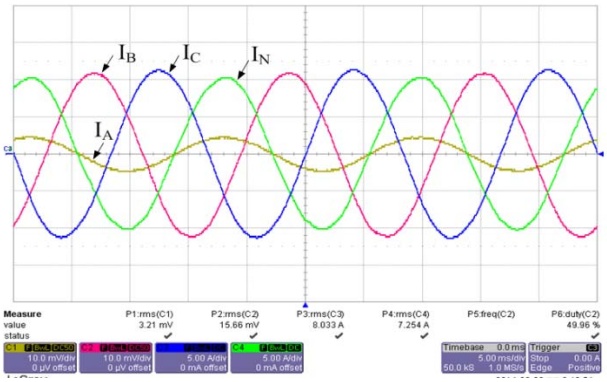

(c) Output load current waveforms with the proposed hybrid controller.

Fig. 13. Output waveforms of the inverter under unbalanced load scenario 1 (10% load on phase A and 100% load on phases B and C).

TABLE IV

DEGREE OF UNBALANCE OF THE THREE-PHASE OUTPUT VOLTAGE IN FIGS. 13 AND 14

Unbalance scenario	Controller	Negative-sequence component (%)	Zero-sequence component (%)
Fig. 13	PI	2.2	5.8
	PI-R	0.1	0.6
Fig. 14	PI	2.2	5.9
	PI-R	0.3	0.5

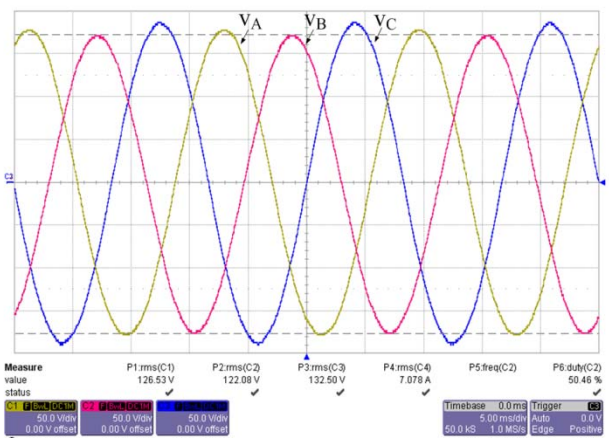

(a) Output phase voltage waveforms with the PI controller.

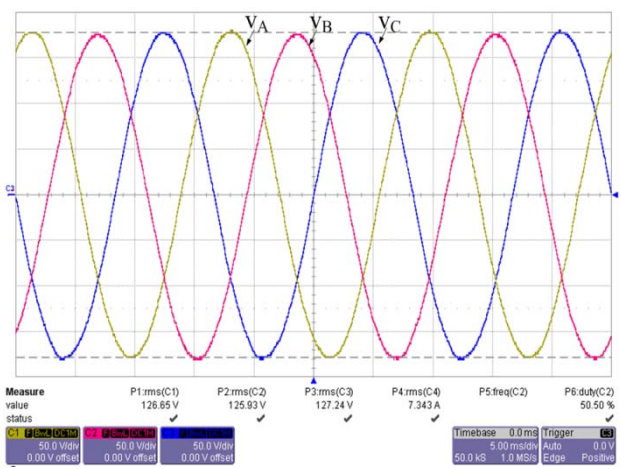

(b) Output phase voltage waveforms with the proposed hybrid controller.

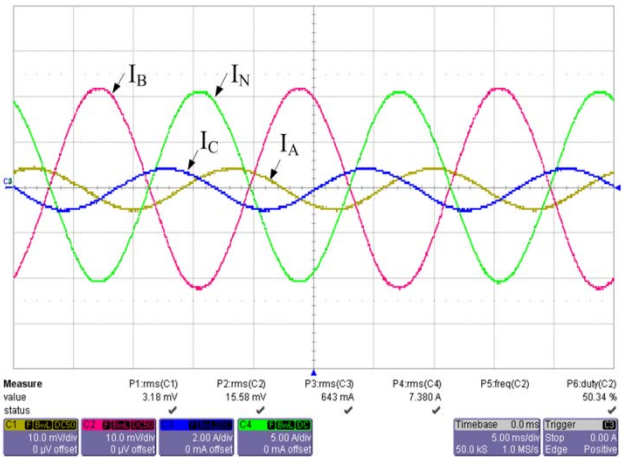

(c) Output load current waveforms with the proposed hybrid controller.

Fig. 14. Output waveforms of the inverter under unbalanced load scenario 2 (10% load on phases A and C and 100% load on phase B).

waveforms of the inverter in the unbalanced load scenario 1 (10% load on phase A and 100% load on Phases B and C). While the three-phase output voltages are not balanced when the conventional PI controller is used, they are clearly balanced when the proposed hybrid controller is applied (Figs. 13(b) and 13(c)).

Another unbalanced load scenario was tested (Fig. 14). In this case, only 10% load was applied to phases A and C, and full load was applied to phase B. While the output waveforms are not balanced with the PI controller (Fig. 14(a)), they are balanced with the proposed hybrid controller (Figs. 14b and 14(c)).

The degree of unbalance of the three-phase output voltage in Figs. 13 and 14 was measured with a Fluke 435 power quality analyzer (Table IV). In both scenarios, the degree of unbalance is less than 0.6%, which is lower than that of methods with symmetric component decomposition (1.2% in [19] and 1.5% in [23]).

V. Conclusions

A hybrid PI + R controller was proposed for the three-phase four-leg inverter to guarantee a balanced output even under unbalanced loads. Using the proposed hybrid controller reduces the complexity of the controller and the calculation amount. The proposed controller is compatible with conventional 3D SVM. The experiment results verify that the proposed controller exhibits excellent performance under unbalanced load conditions. The system is suitable for applications requiring high-quality outputs under unbalanced load conditions.

Acknowledgment

This work was supported by the Soongsil University Research Fund (2013).

References

[1] F. Zhang and Y. Yan, "Selective harmonic elimination PWM control scheme on a three-phase four-leg voltage source inverter," *IEEE Trans. Power Electron.*, Vol. 24, No. 7, pp. 1682-1689, Jul. 2009.

[2] M. V. M. Kumar and M. K. Mishra, "Three-leg inverter-based distribution static compensator topology for compensating unbalanced and non-linear loads," in *IET Power Electron.*, Vol. 8, No. 11, pp. 2076-2084, Nov. 2015.

[3] M. Dai, M. N. Marwali, J. W. Jung, and A. Keyhani, "A three-phase four-wire inverter control technique for a single distributed generation unit in island mode," *IEEE Trans. Power Electron.*, Vol. 23, No. 1, pp. 322-331, Jan. 2008.

[4] U. Borup, F. Blaabjerg, and P. N. Enjeti, "Sharing of nonlinear load in parallel-connected three-phase converters," *IEEE Trans. Ind. Appl.*, Vol. 37, No. 6, pp. 1817-1823, Nov./Dec. 2001.

[5] M. N. Marwali, J.W. Jung, and A. Keyhani. "Control of Distributed Generation Systems Part II: Load Sharing," *IEEE Trans. Power Electron.*, Vol. 19, No. 6, pp. 1551-1561, Nov. 2004.

[6] C. Hongbing, Z. Xing, L. Shengyong, and Y. Shuying, "Research on control strategies for distributed inverters in low voltage micro-grids," *Power Electronics for Distributed Generation Systems (PEDG), 2nd IEEE International Symposium on*, pp. 748-752, 2010.

[7] X. Song, Y. Wang, W. Hu, and Z. Wang, "Three reference frame control scheme of 4-wire grid-connected inverter for microgrid under unbalanced grid voltage conditions," in *Twenty-Fourth Annual IEEE Applied Power Electronics Conference and Exposition*, pp. 1301-1305, 2009.

[8] S. El-Barbari and W. Hofmann, "Digital control of a four leg inverter for standalone photovoltaic systems with unbalanced load," in *Twenty-sixth Annual conference of IEEE, IECON*, pp. 729-734, 2000.

[9] D. Vyawahare and M. Chandorkar, "Distributed generation system with hybrid inverter interfaces for unbalanced loads," *2015 IEEE 6th International Symposium on Power Electronics for Distributed Generation Systems (PEDG)*, Aachen, pp. 1-7, 2015.

[10] R. Kabiri, D. G. Holmes, and B. P. McGrath, "Control of distributed generation systems under unbalanced voltage conditions," *Power Electronics Conference (IPEC-Hiroshima 2014 - ECCE-ASIA), International*, pp. 3306-3313, 2014.

[11] R. Zhang, V. H. Prasad, D. Boroyevich, and F. C. Lee, "Three-dimensional space vector modulation for four-leg voltage-source converters," *IEEE Trans. Power Electron.*, Vol. 17, No. 3, pp. 314-326, May 2002.

[12] N. A. Priya and M. C. Mabel, "Control methods for four-leg voltage source inverter," *International Conference: Devices, Circuits and Systems (ICDCS)*, pp. 44-48, 2012.

[13] E. Demirkutlu, S. Cetinkaya, and A. M. Hava, "Output voltage control of a four-leg inverter based three-phase UPS by means of stationary frame resonant filter banks," *IEEE International Electric Machines & Drives Conference IEMDC '07*, pp. 880-885, 2007.

[14]T. Glasberger and Z. Peroutka, "Control of power supply unit for military vehicles based on four-leg three-phase VSI with proportional-resonant controllers," *13th Power Electronics and Motion Control Conference EPE-PEMC*, pp. 1268-1273, 2008.

[15] H. Chen and J. Min, "Simulation research on the control strategy of three-phase four-leg inverter," *International*

Conference Computer Application and System Modeling (ICCASM), pp. 602-606, 2010.
[16] Y. Hou Zhen and J. Sun, "Study on control strategy for three-phase four-leg inverter power supply," *30th Annual Conference of IEEE Industrial Electronics Society IECON*, pp. 805-809, 2004.
[17] R. Nasiri and A. Radan, "Pole-placement control strategy for 4-leg voltage-source inverters," *1st. Power Electronic & Drive Systems & Technologies Conference (PEDSTC),* pp. 74-79, 2010.
[18]V. Yaramasu, J. Rodriguez, B. Wu, M. Rivera, A. Wilson, and C. Rojas, "A simple and effective solution for superior performance in two-level four-leg voltage source inverters: Predictive voltage control," *IEEE International Symposium Industrial Electronics (ISIE)*, pp. 3127-3132, 2010.
[19]R. A Gannett, J. C. Sozio, and D. Boroyevich, "Application of synchronous and stationary frame controllers for unbalanced and nonlinear load compensation in 4-leg inverters," *Seventeenth Annual IEEE Applied Power Electronics Conference and Exposition, APEC*, pp. 1038-1043, 2002.
[20]K.-H. Kim, N.-J. Park, and D.-S. Hyun, "Advanced synchronous reference frame controller for three-phase UPS powering unbalanced and nonlinear loads," *IEEE 36th Power Electronics Specialists Conference PESC '05*, pp. 1699-1704, 2005.
[21]I. Vechiu, O. Curea, and H. Camblong, "Transient operation of a four-leg inverter for autonomous applications with unbalanced load," *IEEE Trans. Power Electron.*, pp. 399-407, Feb. 2010.
[22]H. Ping and M. Behnke, "A three-phase synchronous frame controller for unbalanced load [invertor operation]," *29th Annual IEEE Power Electronics Specialists Conference*, pp. 1369-1374, 1998.
[23]I. Vechiu, O. Curea, H. Camblong, S. Ceballos, and J. L. Villate, "Digital control of a three-phase four-leg inverter under unbalanced voltage conditions," *European Conference Power Electronics and Applications,* pp. 1-10, 2007.
[24] R. I. Bojoi, G. Griva, V. Bostan, M. Guerriero, F. Farina, and F. Profumo, "Current control strategy for power conditioners using sinusoidal signal integrators in synchronous reference frame," *IEEE Trans. Power Electron.*, Vol. 20, No. 6, pp. 1402-1412, Nov. 2005.
[25]M. Liserre, R. Teodorescu, and F. Blaabjerg, "Multiple harmonics control for three-phase grid converter systems with the use of PI-RES current controller in a rotating frame," *IEEE Trans. Power Electron.*, Vol. 21, No. 3, pp. 836-841, May 2006.
[26]C. Lascu, L. Asiminoaei, I. Boldea, and F. Blaabjerg, "High performance current controller for selective harmonic compensation in active power filters," *IEEE Trans. Power Electron.*, Vol. 22, No. 5, pp. 1826-1835, Sep. 2007.
[27]P. Mattavelli and S. Buso, *Digital Control in Power Electronics*, *1st ed.*, Morgan & Clay Pool Publisher, 2006.
[28]B. C. Choi, *Fundamentals of PWM DC-to-DC Power Conversion*, *2nd ed.*, Young Publishing Co., 2010.
[29] A. Prodic, D. Maksimovic, and R. W. Erickson, "Design and implementation of a digital PWM controller for a high-frequency switching DC-DC power converter," *Industrial Electronics Society IECON*, pp. 893-898, 2001.
[30] A. G. Yepes, F. D. Freijedo, J. Doval-Gandoy, Ó López, J. Malvar, and P. Fernandez-Comesaña, "Effects of discretization methods on the performance of resonant controllers," *IEEE Trans. Power Electron.*, Vol. 25, No. 7, pp. 1692-1712, Jul. 2010.

Van-Tuan Doan was born in Hai Phong, Vietnam, in 1985. He received his B.S. and M.S. degrees in electrical engineering from Vietnam Maritime University, Vietnam, in 2008 and 2012, respectively. He is currently pursuing his Ph.D. degree in electrical engineering at Soongsil University, Republic of Korea. His research interests include DC-DC converters, power factor regulator converters, inverters, and soft-switching techniques for pulse-width modulation converters.

Ki-Young Kim was born in Pohang, Republic of Korea, in 1990. He received his B.S. degree in electrical engineering from Korea National Railroad University, Republic of Korea, in 2014. He is pursuing his M.S. degree at Soongsil University, Republic of Korea. His research interests include DC–DC converters and optimal sizing of the standalone photovoltaic power generation system.

Woojin Choi was born in Seoul, Republic of Korea, in 1967. He received his B.S. and M.S. degrees in electrical engineering from Soongsil University, Republic of Korea, in 1990 and 1995, respectively. He received his Ph.D. degree in electrical engineering from Texas A&M University, USA, in 2004. He worked with Daewoo Heavy Industries as a research engineer from 1995 to 1998. In 2005, he joined the School of Electrical Engineering at Soongsil University. His research interests include modeling and control of electrochemical energy sources (e.g., fuel cells, batteries, and supercapacitors), power-conditioning technologies in renewable energy systems, and DC-DC converters for fuel cells and hybrid electric vehicles. Dr. Choi is an associate editor of IEEE Transactions on Industry Applications and a publication editor of the Journal of Power Electronics of the Korean Institute of Power Electronics.

Dae-Wook Kim was born in Seoul, Republic of Korea, in 1973. He received his B.A. in economics from Yonsei University, Republic of Korea, in 1999. He received his Ph.D. degree in economics from University of California at Davis, USA, in 2004. From 2004 to 2007, he worked for Korea Institute for Industrial Economics and Trade as a research fellow. In 2007, he joined the Department of Economics of Soongsil University. His current research interests include energy economics, with particular interest on market structure and competition, in energy industries.